COMPUTATION OF SUPERSONIC FLOW AROUND THREE-DIMENSIONAL WINGS

B. G. Arlinger

Saab-Scania, Linköping, Sweden

Abstract

As part of the development of a program for supersonic flow around realistic aircraft configurations a method is presented for the computation of strictly supersonic flow around single wings or two-wing configurations of arbitrary shape.

The method is based on the steady Euler equations which are solved in a streamwise marching procedure using a shock-capturing finite volume formulation. As solution algorithm an explicit predictor-corrector scheme of MacCormack type is used.

A variety of numerical applications of the method is presented including canard configuration cases, and comparisons are made with other theories and test data confirming versatility and reliability of the method.

1. Introduction

Various methods exist today for the computation of three-dimensional steady supersonic flow, ranging from panel methods to finite difference and characteristic methods. The panel methods are based on linear theory and are in many cases clearly insufficient tools even when improved by higher-order corrections[1,2].

Among the finite difference methods for supersonic flow, the majority are based on the Euler equations to get rid of limitations on shock strength, etc. However, for low supersonic Mach numbers where the shock waves are relatively weak, the transonic finite difference programs developed for the non-linear potential equation can be a good alternative after some modification to improve the convergence. In this speed regime where subsonic regions still exist, the marching Euler codes can not be used and the time-dependent Euler codes are much more time-consuming than the potential programs.

Also for higher supersonic speeds a non-linear potential method has proven very effective[3], provided the Mach number normal to all shock waves is less than around 1.4.

However, for strictly supersonic flow, methods based on the steady Euler equations seem to be the best candidates for a flexible and cost-effective tool for the aerodynamicist. The existing finite difference methods of this type could be subdivided in two groups depending on the treatment of shock waves. For rather simple configurations (e.g. similar to a smoothed space shuttle) accurate solutions to the steady Euler equations can be obtained using a shock fitting technique where grid surfaces in the mesh are forced to coincide with shock surfaces[4,5]. On the other hand, more generally applicable codes could be written based on shock capturing technique, but to the cost of degraded resolution of the discontinuites of the flow. Methods of the latter type[6-8] have been applied to various configurations, however still rather simple compared to typical aircraft shapes.

Although codes based on the equations written in characteristic coordinates can give very accurate shock wave predictions, they lack the versatility and computational efficiency of shock-capturing finite difference methods[9].

The present work is part of an effort to develop a program for marching solution of the steady Euler equations applicable to realistic aircraft configurations. Shock capturing technique was therefore chosen and the computational grid should be adaptable to wings and bodies of various shapes. As a first step the computation of the flow around three-dimensional wings without a body has been studied and is presented here. The chosen grid is simple and can be extended to suit also bodies. The solution is advanced between planes normal to the free stream direction using a predictor-corrector scheme of the MacCormack type[10] for a finite volume formulation of the steady Euler equations. The maximum allowable step size is controlled by the Courant-Friedrichs-Lewy stability criterion.

Because the grid is not aligned with the leading or trailing edges, the program is very general and can handle any type of wing planforms and combination of wings, provided the flow speed in the marching direction is supersonic everywhere. Wings with any degree of leading edge bluntness can thus be handled as long as $M_\infty \sin^2\Lambda > 1$, where Λ is the leading edge sweep angle. For lower Mach numbers or sweep angles the method works as long as the typical bluntness scale is only a minor fraction of the mesh height. To get higher resolution in these cases a small modification to local wedge-like leading edges is very effective, and has only a local influence on the pressure distribution.

The computational results presented here show good agreement with linear theory for small disturbance cases, and with non-linear methods and experiments. The versatility of the method is illustrated by computations for single wings and canard configurations both with forward and backward swept wings.

2. Mathematical formulation

The equations expressing the conservation of mass and momentum are, written in Cartesian coordinates

$$\frac{\partial \bar{F}}{\partial x} + \frac{\partial \bar{G}}{\partial y} + \frac{\partial \bar{H}}{\partial z} = 0 \ , \qquad (1)$$

where $\bar{F}$, $\bar{G}$ and $\bar{H}$ are the column vectors

$$\bar{F} = \begin{pmatrix} \rho u \\ \rho u^2+p \\ \rho uv \\ \rho uw \end{pmatrix} \quad \bar{G} = \begin{pmatrix} \rho v \\ \rho vu \\ \rho v^2+p \\ \rho vw \end{pmatrix} \quad \bar{H} = \begin{pmatrix} \rho w \\ \rho wu \\ \rho wv \\ \rho w^2+p \end{pmatrix} \qquad (2)$$

Here u,v,w are the velocity components in the x,y and z directions, and p and ρ are the pressure and the density.

In steady flow the energy conservation equation may be integrated to

$$\frac{\gamma}{\gamma-1}\frac{p}{\rho} + \frac{u^2+v^2+w^2}{2} = h_o \qquad (3)$$

where γ is the specific heat ratio and h_o is the stagnation enthalpy, constant in the whole flow field for uniform upstream flow.

For strictly supersonic flow the five equations (1) and (3) constitute a hyperbolic system of first order partial differential equations for the five unknowns u,v,w,p and ρ , which is solved by marching in the x-direction.

The finite volume formulation used for the numerical solution of Eqs. (1) is based on the integral form of these equations, obtained by applying Gauss' theorem,

$$\iint \bar{\bar{T}} \cdot d\bar{S} = 0 \qquad (4)$$

where $\bar{\bar{T}}$ is the second order tensor $(\bar{F},\bar{G},\bar{H})$, $d\bar{S}$ is the surface element vector, normal to the surface, and the integral can be taken over any closed surface in the flow. For instance, the surface can be the six faces of a cell of arbitrary shape which maps to a cube in a transformed space spanned by the coordinates x^1, x^2, x^3. Denoting the surface element vector of each face by $d\bar{S}^m$, Eq. (4) obviously becomes

$$\sum_{m=1}^{6} \iint \bar{\bar{T}} \cdot d\bar{S}^m = 0 \qquad (5)$$

Using standard tensor formalism this equation can be retransformed into the differential form

$$\iiint \frac{1}{\sqrt{g}} \frac{\partial}{\partial x^i} (\sqrt{g}\, \bar{\bar{T}} \cdot \bar{g}^i) dV = 0 \qquad (6)$$

where the volume integral is taken over the physical cell. $\sqrt{g}$ is the Jacobian $\partial(x,y,z)/\partial(x^1,x^2,x^3)$, $\bar{g}^i$ is the contravariant base vector[11] grad x^i, dV is the physical volume element and repeated indices are summed. The integrand in Eq. (6) is the expression for the divergence of the tensor $\bar{\bar{T}}$ in an arbitrary curvilinear system, as it should be. The mathematical identity between Eqs. (5) and (6) should be recalled when comparing integral and differential formulations on curvilinear grids, as pointed out also by Rizzi et al[8].

3. Numerical procedures

Computational grid

Because the present wing program will be developed further towards a general program applicable to a variety of aircraft configurations, the grid system chosen for the wing problem is simple and general. The solution is advanced between planes normal to the free stream direction, which coincides with the x-axis. In these planes the vertical grid lines, parallell to the z-axis, are uniformly distributed, and the other grid lines adapt to the wing surfaces as illustrated in Fig. 1. The leading and trailing edges of each wing always lie in a grid surface, and in the present form the wing tips have to coincide with planes of constant y.

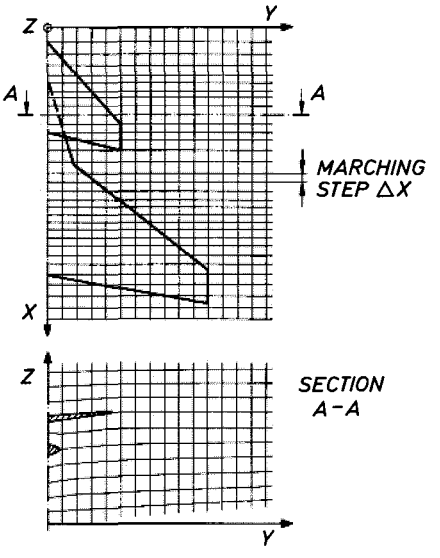

Fig 1. Type of grid used for a wing configuration

The wings can have any type of thickness, camber and twist distribution, and for each marching step the length of which is determined by a stability condition, the grid in the new y,z plane is generated and defines, together with the grid in the previous plane, the cells used in the finite volume algorithm.

The extension of the computational region in the y and z directions is chosen for each case so that unwanted signal reflections from the grid outer surfaces are avoided.

Marching algorithm

The mass and momentum flow equations (5) are applied on an elementary volume with plane end surfaces normal to the x-axis and with the nodes in the middle of these, Fig. 2. For generality the 4 side surfaces are assumed non-planar although in the present program two of them are plane and parallell (y=constant). Denoting the surface vectors of the 4 side surfaces as indicated in Fig. 2, Eq. (5) can be discretized according to the following two-step scheme of MacCormack type[10], where, for clarity, the bars on F and T have been omitted,

$$\tilde{F}_{jk}^{n+1} S_{2x} = F_{jk}^{n} S_{1x} - T_{j+r,k}^{n} \cdot \bar{S}_{2y} - T_{j+r-1,k}^{n} \cdot \bar{S}_{1y} - T_{j,k+s}^{n} \cdot \bar{S}_{2z} - T_{j,k+s-1}^{n} \cdot \bar{S}_{1z} \qquad (7a)$$

$$F_{jk}^{n+1} S_{2x} = \frac{1}{2}\left[\tilde{F}_{jk}^{n+1} S_{2x} + F_{jk}^{n} S_{1x} - \tilde{T}_{j-r+1,k}^{n+1} \cdot \bar{S}_{2y} - \tilde{T}_{j-r,k}^{n+1} \cdot \bar{S}_{1y} - \tilde{T}_{j,k-s+1}^{n+1} \cdot \bar{S}_{2z} - \tilde{T}_{j,k-s}^{n+1} \cdot \bar{S}_{1z}\right] \qquad (7b)$$

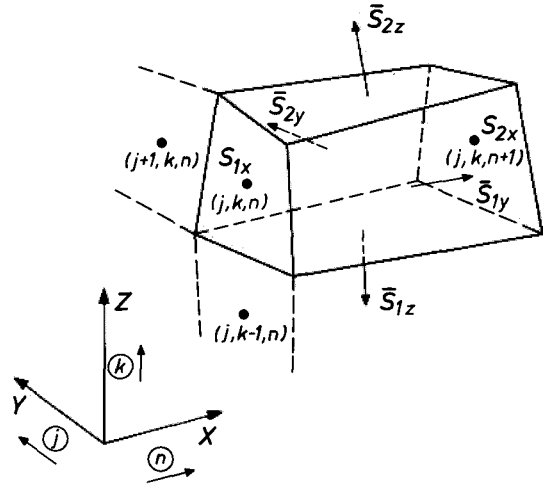

Fig 2. The computational cell

The subscripts j and k are cell indices in the y and z directions respectively, while r and s are chosen equal to 1 or 0. The latter indices control the 4 possible asymmetry combinations in the MacCormack scheme, and are free to choice by the program runner. The areas of the two end surfaces are S_{1x} and S_{2x}, lying in the x-planes indicated by the superscripts n and n+1, and each surface vector of the cell side surfaces has the area projections in the x,y and z directions as components.

As follows from applying Eq. (6) to a uniform grid in the x^i-space and from the identity between Eq. (5) and Eq. (6), the difference scheme (7) is second order accurate. This holds for an arbitrary curvilinear grid that maps smoothly to a uniform grid in the transformed space, provided the nodes on the physical elementary volumes map to the midpoints of the corresponding surfaces of the cubes in the transformed space.

The application of the predictor-corrector scheme (7) yields the $\bar{F}$ field at level n+1, from which the five physical quantities and $\bar{G}$ and $\bar{H}$ are obtained by combining the definition of $\bar{F}$ in Eq. (2) and the energy equation (3). Denoting the 4 components of $\bar{F}$ by F_i the relations are

$$v = \frac{F_3}{F_1}$$

$$w = \frac{F_4}{F_1}$$

$$u = \frac{\gamma}{\gamma+1}\left\{\frac{F_2}{F_1} + \left[\left(\frac{F_2}{F_1}\right)^2 - 2\,\frac{\gamma^2-1}{\gamma^2}\left(h_o - \frac{v^2+w^2}{2}\right)\right]^{1/2}\right\} \qquad (8)$$

$$\rho = \frac{F_1}{u}$$

$$p = \frac{\gamma-1}{\gamma}\,\rho\left(h_o - \frac{u^2+v^2+w^2}{2}\right)$$

Viscosity

Writing the modified equation for the MacCormack scheme applied to a simple scalar equation, shows that the leading extra terms (for Courant numbers < 1) are a second order dispersive and a third order dissipative term[6]. This indicates the possible need for an extra dissipative term to damp oscillations. Thus, a case with pressure fluctuations close to a leading edge led to the introduction of an artificial viscosity term in the marching algorithm as an option. It is applied only in the corrector step, Eq. (7b), to which the following term is added on the right hand side

$$\mu\,\frac{\Delta x\Delta y}{100}\left(F^n_{j+1,k} + F^n_{j-1,k} + F^n_{j,k+1} + F^n_{j,k-1} - 4F^n_{jk}\right)$$

where μ is a viscosity coefficient and Δx and Δy are the cell dimensions in the x and y directions.

If a uniform quadratic grid is thought of in the y,z plane the modified algorithm solves the equation

$$F_x + G_y + H_z = \mu\,\frac{\Delta y}{100}\,(F_{yy} + F_{zz})$$

Values of μ found to be effective without too much smoothing of shock waves were of the order 0.05 L/Δy, with L as a typical spanwise dimension, say half the wing span.

Most cases were run with good results keeping μ=0.

Stability

The marching step size has to be smaller than a limit set by the Courant-Friedrich-Lewy criterion. Applying the formulation that the finite difference domain of influence at least must include the continuum domain of influence yields the following two conditions on Δx:

$$\Delta x \leq (u^2+w^2-c^2)\,\Delta y \Big/ \Big\{k_y(u^2+w^2-c^2) - uv - vwk_z + (q^2-c^2)^{1/2}\left[c^2(1+k_z^2) - (uk_z-w)^2\right]^{1/2}\Big\} \qquad (9a)$$

$$\Delta x \leq (u^2+v^2-c^2)\,\Delta z \Big/ \Big\{k_z(u^2+v^2-c^2) - uw - vwk_y + (q^2-c^2)^{1/2}\left[c^2(1+k_y^2) - (uk_y-v)^2\right]^{1/2}\Big\} \qquad (9b)$$

where $q^2=u^2+v^2+w^2$ and c is the local speed of sound. In deriving these conditions the cell is approximated by a parallellepiped with rectangular cross section of measure Δy times Δz and with a slope relative to the x-axis defined by the vector (1, k_y, k_z).

At present a simplified version of Eqs.(9) is used in the program, obtained by setting w and k_z equal to zero in the first equation and v and k_y equal to zero in the second, corresponding to a two-dimensional stability analysis in the x,y and x,z planes. Recalling that k_y is equal to zero in the present grid the actual expressions used are

$$\Delta x \leq \frac{(u^2-c^2)\,\Delta y}{-uv+c\,(u^2+v^2-c^2)^{1/2}} \equiv \Delta x_{m,y} \qquad (10a)$$

$$\Delta x \leq \frac{(u^2-c^2)\,\Delta z}{k_z\,(u^2-c^2)-uw+c\,(u^2+w^2-c^2)^{1/2}} \equiv \Delta x_{m,z} \qquad (10b)$$

Each new marching step is computed from the relation

$$\Delta x = C \min(\Delta x_{m,y}, \Delta x_{m,z}) \qquad (11)$$

where the minimum for the whole of the latest y,z plane is sought for. A suitable value for the constant C was found to be about 0.8.

Boundary conditions

Wing surface

At a cell side coinciding with a wing surface the no-flow condition implies that the corresponding terms in Eqs. (7) of the type $\bar{\bar{T}}\cdot\bar{S}_z$ are reduced to

$$p_w \begin{pmatrix} 0 \\ S_{zx} \\ S_{zy} \\ S_{zz} \end{pmatrix} \qquad (12)$$

where p_w is the wing surface pressure and the surface area vector $\bar{S}_z$ is

$$\bar{S}_z = [S_{zx},\ S_{zy},\ S_{zz}]. \qquad (13)$$

Thus p_w^n and $\tilde{p}_w^{n+1}$ are needed in the predictor and corrector respectively for a cell adjacent to a wing surface. Because there are no nodes on the wing surface, these pressure values have to be calculated from the flow field variables at the nodes half a cell height from the surface.

Here a characteristics relation is used for this calculation. A general three-dimensional compatibility relation in a plane containing the velocity vector may be written

$$\frac{\partial p}{\partial \xi^{\pm}} \pm \frac{\rho u'^2}{\beta} \frac{\partial}{\partial \xi^{\pm}} \left(\frac{w'}{u'}\right) + \frac{\rho c}{\beta} \frac{\partial v'}{\partial \eta} = 0 \qquad (14)$$

where ξ^+ and ξ^- are the two bicharacteristics in the plane, η denotes a direction normal to the plane, u' and w' are any two orthogonal velocity components in the plane, v' is the velocity component in the normal direction η and thus equal to zero in the plane, and $\beta = [(u'^2+w'^2)/c^2-1]^{1/2}$. The two bicharacteristic directions have the slopes

$$\frac{u'w' \pm \beta c^2}{u'^2-c^2}$$

relative to the u' direction.

For the present purpose an x,z plane through the relevant nodes is considered, see Fig. 3a. If, for simplicity, the normal derivative term of Eq. (14) is neglected, a finite difference relation along the ξ^- characteristic may be written as

$$p_W = p_A + \left(\frac{\rho u'^2}{\beta}\right)_A \left[0-\left(\frac{w'}{u'}\right)_A\right] \qquad (15)$$

where subscripts W and A refer to the corresponding points in Fig. 3a, and the u' direction is chosen parallell to the surface slope in the wall point W. The location of point A and the physical state there can be determined in an iterative sequence utilizing the points N and N+1 and the slope of the ξ^- characteristic.

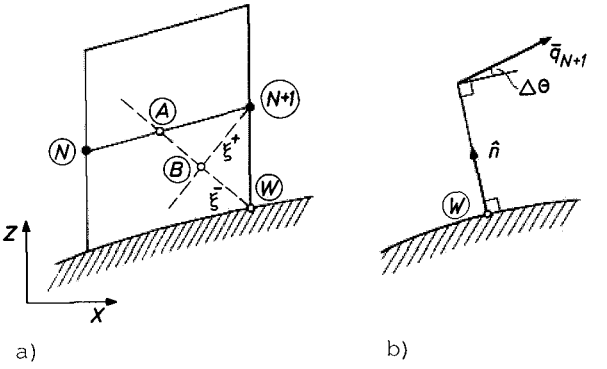

a) b)

Fig 3 a) Bicharacteristics for compatibility relation close to wing surface

b) $\hat{n}$, $\bar{q}_{N+1}$ plane for finite difference formulation of compatibility relation

It was found, however, that improved results, in the form of clearly reduced pressure oscillations after abrupt changes in contour slope, were obtained if the state at point N+1 was used in Eq. (15) instead of point A. This is equivalent to the assumption that the ξ^+ characteristics are simple waves, implying the same physical state at point B and N+1, and thus replacing the point A with the point B along the same characteristic.

The latter version of boundary condition was chosen for the present program and is in a sense similar to the Abbett[12] method applied to grids with nodes on the wall.

The actual difference relation used is written for the plane defined by the surface unit normal $\hat{n}$ in the wall point and the velocity vector $\bar{q}$ in the point N+1, see Fig. 3b. With the u' direction as the surface tangent in the wall point the relation obtained from Eq. (14) without its third term is

$$p_W = p_{N+1} - \left(\frac{\rho q^2 \cos^2 \Delta\theta}{\beta} \tan \Delta\theta\right)_{N+1} \qquad (16)$$

where the difference in flow direction between the points N+1 and W, $\Delta\theta$, is obtained from

$$\bar{q}_{N+1}\cdot\hat{n} = |\bar{q}_{N+1}| \sin \Delta\theta \qquad (17)$$

Leading and trailing edge regions

In the leading and trailing edge regions of a wing there are cells the bottom or top surfaces of which contain both wing surface and area open to flow. The corresponding terms in Eqs. (7) of the form $\bar{\bar{T}}\cdot\bar{S}_z$ then are divided in a flow part and a wing surface part indicated by subscripts F and W respectively, resulting in

$$\bar{\bar{T}}\cdot\bar{S}_z=\rho\bar{q}\cdot\bar{S}_{Fz}\begin{pmatrix}1\\u\\v\\w\end{pmatrix}+p_F\begin{pmatrix}0\\S_{Fzx}\\S_{Fzy}\\S_{Fzz}\end{pmatrix}+p_W\begin{pmatrix}0\\S_{Wzx}\\S_{Wzy}\\S_{Wzz}\end{pmatrix} \qquad (18)$$

The area vector $\bar{S}_z$ is thus replaced by the two area vectors

$$\bar{S}_{Fz} = [S_{Fzx}, S_{Fzy}, S_{Fzz}]$$

$$\bar{S}_{Wz} = [S_{Wzx}, S_{Wzy}, S_{Wzz}]$$

For the flow variables mean values are used between the node values above and below the cell surface, and also a spanwise interpolation is made depending on the amount of sweep of the wing edge. When computing the pressure p_W at the wing surface part, the procedure based on a compatibility relation, presented above, is used with some modifications. For example, the local surface normal is taken at the center of gravity of the wing area part.

Outer surfaces

A computational box is determined before running the program by prescribing the top and bottom values of z and the maximum spanwise coordinate y. The boundary conditions applied at these surfaces imply zero normal gradients of all physical variables.

The cells that are processed at each marching step normally do not cover the whole computational area until after a certain x distance, because the program only considers those cells that fall within the wing-generated Mach cones plus some margin.

At the plane y=0 image nodes are used on the negative y side with symmetrically assigned values of the pressure and density and the velocity vector.

4. Computational results

A great number of very different configurations have been run with the present program.

First some two-dimensional calculations are presented to get clear and simple comparisons with exact and linear theory results. Thus Fig. 4 shows the computed pressure distribution for a 15 % thick double wedge at M_∞ =2.0. The agreement with exact theory is perfect, and the pressure discontinuities are captured quite well.

In Fig. 5 computed wave drag values are presented for two series of double wedges at M_∞=2.0. The drag values for the 1 % thick double wedge is seen to agree very well with linear theory, while the results for the 15 % thick double wedge illustrate the non-linear thickness effects on drag.

Most wave drag calculations for three-dimensional configurations are based on linear theories. To get a comparison of drag results from the present method with an established linear drag curve, a swept wing with a parabolic arc profile was calculated. Fig. 6 presents the thickness-scaled wave drag as a function of Mach number, where the linear theory curve[13] has the typical peak value for sonic leading and trailing edges at M_∞ =1.8. To get a good comparison with linear theory, calculations were made with the present method for a 1 % thick version of the wing with a grid having Δy and Δz equal to 2.5 % of the root chord. The resulting drag values are seen to be in good agreement with linear theory for supersonic leading edge cases, but the sonic leading edge value is lower and the results for subsonic leading edge cases are higher than linear theory. The difference in peak value is due partly to insufficient resolution in the grid of the large pressure gradients close to the leading edge, but also to the fact that linear theory is not valid locally at the leading edge in case this is sonic. It gives a pressure that tends to infinity with the inverse square root of the distance to the leading edge. For a subsonic leading edge case the pressure singularity in linear theory is weaker (logarithmic in the distance to the leading edge), but for Mach numbers approaching 1 the relative importance of the neglected non-linear terms increase.

Computations made with the same grid for a 10 % thick version of the wing are seen to give almost no drag peak when passing from subsonic to supersonic leading edge.

Some linear theory pressure distributions are presented in Fig. 7 for a single-wedge delta[14], illustrating the pressure singularities at the leading edge for subsonic and sonic leading edges. The present method results for a wedge slope of 0.5 % show good agreement with the linear theory.

To illustrate a simple lifting case Fig. 8 shows two spanwise pressure distributions for a thin planar swept wing at Mach number 1.5. The angle of attack, 3°, is sufficiently high to give a weak asymmetry in the upper and lower side pressure curves, and also a small suction peak at the tip due to crossflow around it.

A case with strong non-linear effects can be obtained when the flow is transonic normal to the leading edge for a lifting configuration. In Fig. 9 a spanwise pressure distribution for such a case is shown. The 70° swept delta has a NACA 65A003 profile, and for M_∞ =2.0 and $\alpha=6^\circ$ a cross-flow shock wave stands close to the leading edge. This case has been calculated by Grossman and Siclari[3] using their non-linear potential method, which has a grid with very high resolution in the leading edge region. The present method, which has an essentially uniform grid, is seen to give results in close agreement with the cited method except for a small suction peak that is not captured by the present grid.

The oscillations behind the shock are typical for Euler equation solutions with the MacCormack scheme, and they can be effectively suppressed by giving the viscosity coefficient μ a suitably high value. In the present case a μ value of around 3 was sufficient to damp out the wiggles, but μ=1 was chosen in the calculation shown here to avoid the accompanying shock smearing effects.

The asymmetry indices r and s in Eqs. (7) are also known to have some effect on oscillations in connection with shock waves. The r value of 1 used here (s=0) gave slightly weaker oscillations than r=0, which seems to be in accordance with previous observations[6].

A comparison with wind tunnel results[15] is shown in Fig. 10 where pressure distributions are given for a 70^{o} swept delta with a 6 % thick circular arc airfoil at $M_{\infty}=1.465$ and $\alpha=2^{o}$. The agreement between theory and experiment is quite good apart from the outboard suction peak in the experimental pressure, which probably is due to a leading edge vortex.

To illustrate the flexibility of the present method some results for a canard configuration similar to that of Saab 37 Viggen are given in the next two figures. The canard is located above the main wing plane and is set at a positive angle of incidence relative to it. In Fig. 11 pressure distributions are shown for the case $M_{\infty}=1.4$, $\alpha=2^{o}$, calculated with the present method and with a transonic small perturbation potential method (TSP) modified to work also for supersonic free stream flow[16]. For the present method calculations the inner part of the main wing was modified smoothly over the first 15 % of the local chord to get a wedge-like airfoil nose instead of the original blunt nose. This was done to avoid getting too many subsonic points in the calculations at this relatively low Mach number. The program does not stop for a subsonic point (it is skipped over in the marching step calculation), but the result will be more or less influenced locally. In the relatively coarse grid used here to match the potential solution (Δy and Δz=3.8 % of the main wing root chord), 1 subsonic point was obtained for the modified geometry and 12 for the original.

Disregarding the minor difference in the geometry used by the two methods, and the fact that one of the conditions for the validity of the TSP equation is that the Mach number is close to 1.0, the results may be compared and are seen to agree quite well. A characteristic difference seems to be a slight suction peak in the Euler method results close to the leading edge, which is not seen in the potential method pressures.

A run made with the same grid but at $M_{\infty}=2.0$, $\alpha=2^{o}$ and for the unmodified geometry, is presented in Fig. 12.

Finally, some results are given for a canard configuration with a forward swept wing, designed only as a computational test object. The airfoil thickness distribution for both wings is a NACA 65A004 with a smoothly modified nose over the first 15 % of the chord to a wedge with half angle 8^{o} at the nose. A NACA mean line with a=0.5 was used for cambering the airfoils.

In Figs. 13 and 14 pressure distributions for the case $M_{\infty}=1.8$, $\alpha=2^{o}$ are shown for both the canard-wing and wing alone configuration. The canard is seen to slightly decrease the loading on the inner part of the wing and increase it just outside the canard tip.

Figs. 15a-c illustrate the computed pressure fields in three planes normal to the flow for the case in Fig. 13. One detail seen in these patterns are the two distinct pressure maximas above and below the wing in Fig. 15c. They are the result of interference between the two wave surfaces generated by the leading edge parts inside and outside of the corner.

The mesh used in all calculations for the forward swept wing had a Δy=1.78 % of the main wing root chord and a Δz varying slightly around the same value. The added viscosity term was kept small by using $\mu=1$.

As example of running times the case in Fig. 13 required 25.7 CPU minutes on a VAX 11/780 using around $0.70 \cdot 10^{6}$ grid points (maximum 11520 points were used in each y,z plane and 125 marching steps were required). For the same number of grid points a fully converged solution of the time-dependent Euler equations would have required orders of magnitude more computer time (~100-1000 times more), illustrating the effectiveness of the marching technique in strictly supersonic flow.

5. Concluding remarks

By using a simple, almost uniform grid that adapts to the wing surfaces but not to the wing planform in the form of aligning or refinement close to the wing edges, a very flexible program has been obtained for the computation of strictly supersonic flow around arbitrary wing configurations. The somewhat decreased resolution of flow details close to leading edges compared to more specialized and restricted methods has only local effect. In fact, the very high cost-effectiveness of marching methods compared to iterative methods for the Euler equations favours the use of very fine grids giving a high resolution in most areas. Grid stretching in the y and z directions in the outer part of the computational region also simplifies the econimizing of grid points.

The next step along the development line started by the present method is a marching program for bodies of arbitrary shape. That work is just recently completed yielding very good results. The present wing program will next be developed to suit the body program grid in order to have a general wing-body code for real aircraft configurations.

References

1. Ehlers,F.E., Epton,M.A., Johnson,F.T. and Rubbert,P.E., "An Improved Higher-Order Panel Method for Linearized Supersonic Flow", AIAA Paper No 78-15, Jan 1978.

2. Mason,W.H. and DaForno,G., "Opportunities for Supersonic Performance Gains Through Non-Linear Aerodynamics", AIAA Paper No 79-1527, July 1979.

3. Grossman,B. and Siclari,M.J., "The Non-Linear Supersonic Potential Flow over Delta Wings", AIAA Paper No 80-0269, Jan 1980.

4. Marconi,F. and Siclari,M.J., "A Study of the Inviscid Flow about Conically Cambered Delta Wings", AIAA Paper No 78-58, Jan 1978.

5. Marconi,F. and Koch,F., "An Improved Supersonic Three-Dimensional, External, Inviscid Flow Field Code", NASA CR 3108, 1979.

6. Kutler,P., Lomax,H. and Warming,R.F., "Computation of Space Shuttle Flow Fields Using Non-centered Finite-Difference Schemes", AIAA J., Vol 11, No 2, pp. 196-204, Feb 1973.

7. Kutler,P., "Computation of Three-Dimensional Inviscid Supersonic Flows", in Progress in Numerical Fluid Dynamics, Lecture Notes in Physics, Vol 41, Springer-Verlag, Berlin, 1975, pp. 287-374.

8. Rizzi,A.W., Klavins,A. and MacCormack,R.W., "A Generalized Hyperbolic Marching Technique for Three-Dimensional Supersonic Flow with Shocks", in Proc. Fourth Int. Conf. on Num. Methods in Fluid Dynamics, Lecture Notes in Physics 35, Springer-Verlag, 1975, pp. 341-346.

9. Rakich,J.V. and Kutler,P., "Comparison of Characteristics and Shock Capturing Methods with Application to the Space Shuttle Vehicle", AIAA Paper No 72-191, Jan 1972.

10. MacCormack,R.W., "Numerical Solution of the Interaction of a Shock Wave with a Laminar Boundary Layer", Proc. Second Int. Conf. on Num. Methods in Fluid Dynamics, Springer-Verlag, Berlin, 1971, pp. 151-163.

11. Rutherford,A., "Vectors, Tensors, and the Basic Equations of Fluid Mechanics", Prentice-Hall, Englewood Cliffs, N.J., 1962.

12. Abbett,M.J., "Boundary Condition Computational Procedures for Inviscid Supersonic Steady Flow Field Calculations", Aerotherm Corp., Mt. View, Calif., Final Rept. 71-41, 1971.

13. Engineering Sciences Data, Aerodynamic Sub-Series Vol 2a, Aerodynamics of Wings and Aerofoil Sections, W.S. 02.03.01, 1957.

14. Pucket,A.E., "Supersonic Wave Drag of Thin Airfoils", J. Aero. Sci, Vol 13, No 9, p 475, 1946.

15. Larsson,P.O., "Tryckfördelningsmätning på 70° deltavingar med olika profilform vid överljudhastighet", FFA Rapport AU-232, 1953.

16. Agrell,N. and Hedman,S.G., "Calculations of Transonic Steady State Aeroelastic Effects for a Canard Airplane", ICAS-82-2.1.2, Seattle, 1982.

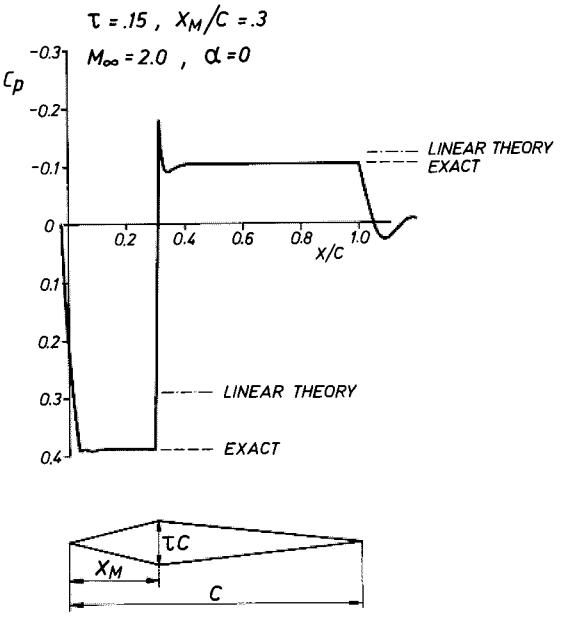

Fig 4. Pressure distribution for double wedge calculated with present method

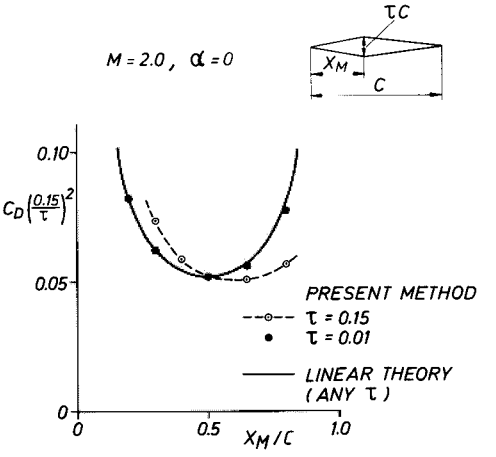

Fig 5. Double wedge wave drag as function of maximum thickness position

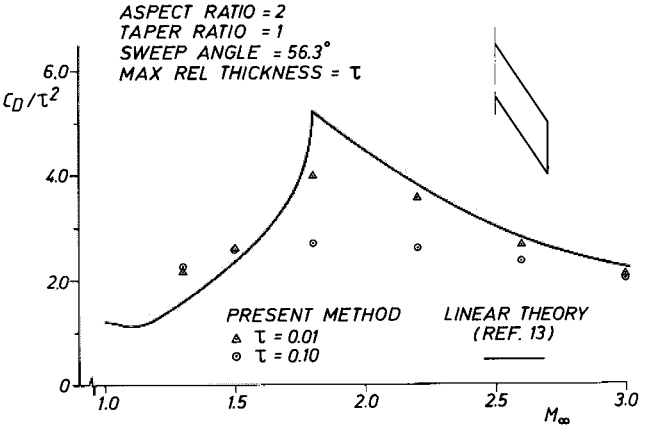

Fig 6. Wave drag for swept wing with parabolic arc profile at α=0

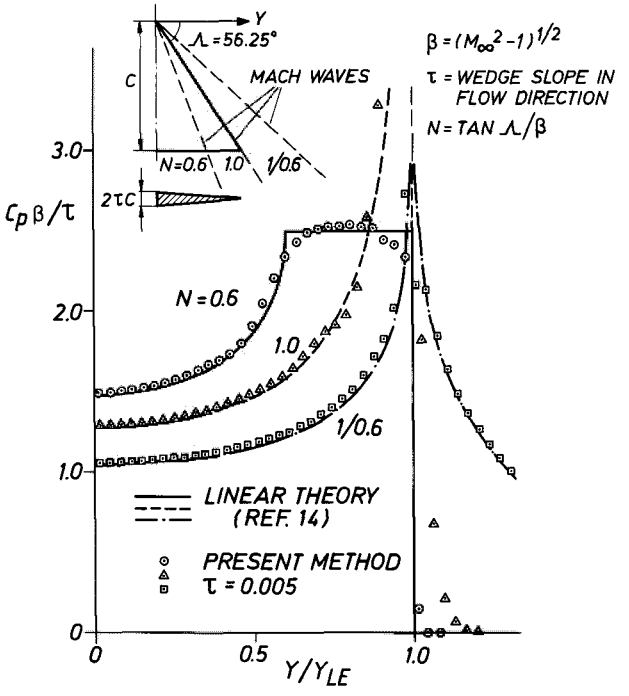

Fig 7. Pressure coefficient parameter for single-wedge delta at $\alpha=0$

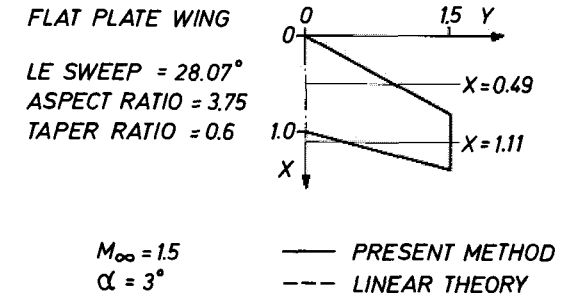

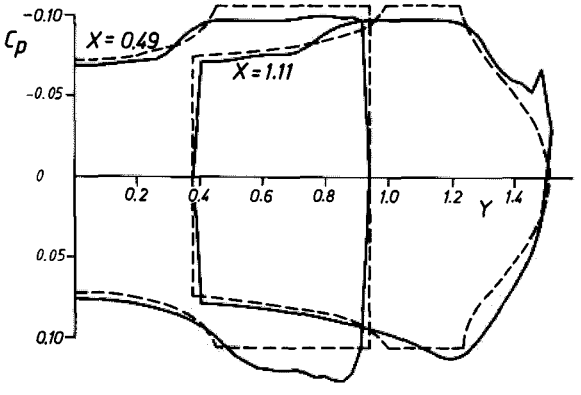

Fig 8. Spanwise pressure distributions for thin swept wing

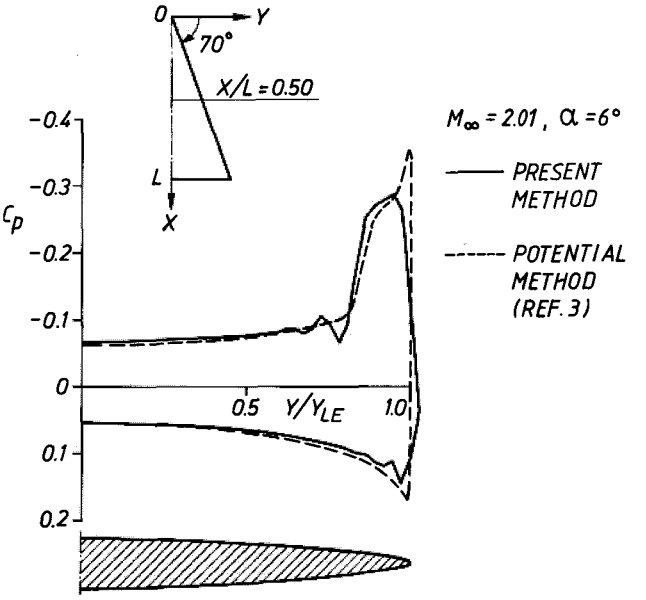

Fig 9. Calculated cross flow pressure distribution at x/L=0.5 on delta wing

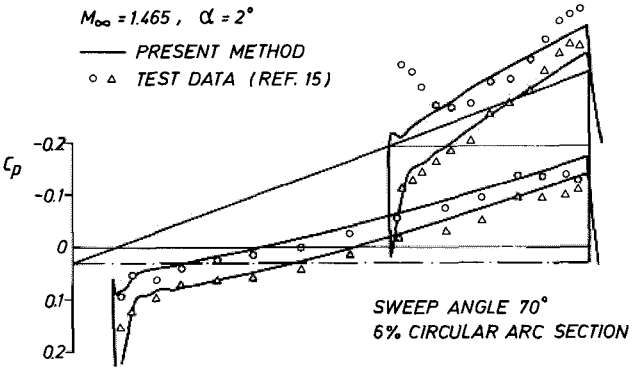

Fig 10. Calculated and experimental pressure distributions for delta wing

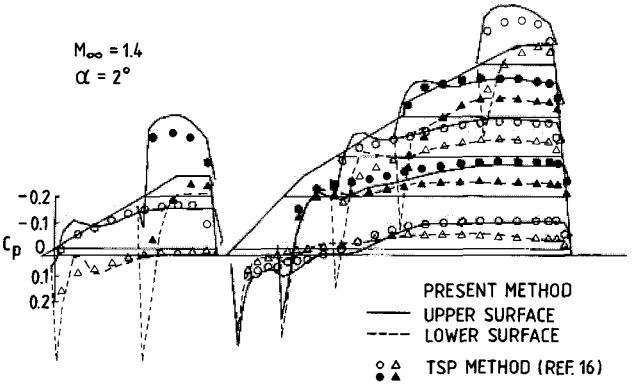

Fig 11. Calculated pressure distribution for canard configuration

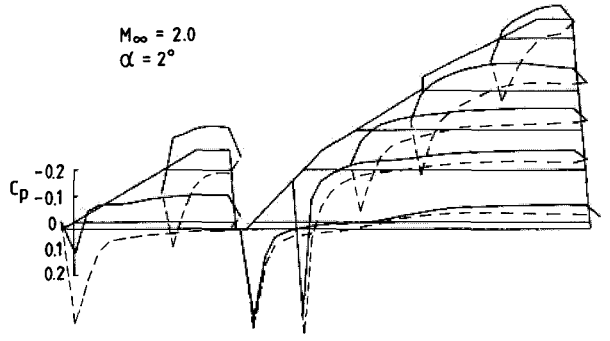

Fig 12. Present method result for canard configuration

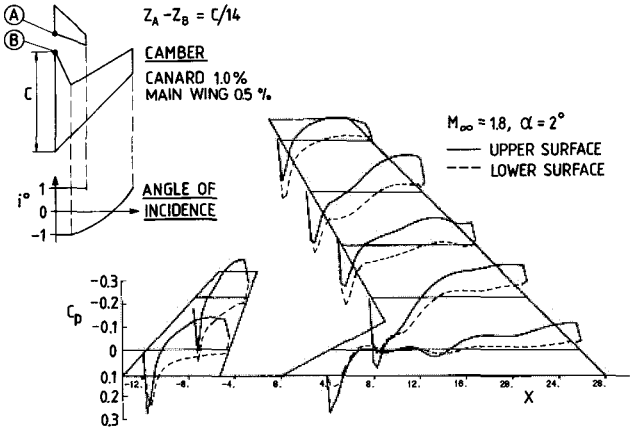

Fig 13. Pressure distribution for forward-swept wing with canard

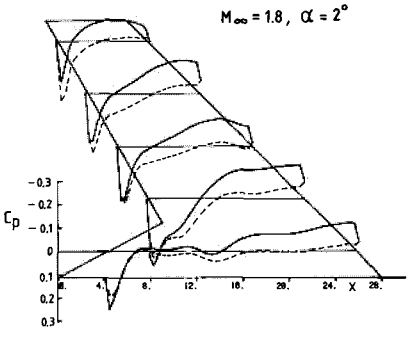

Fig 14. Pressure distribution for forward-swept wing (canard off)

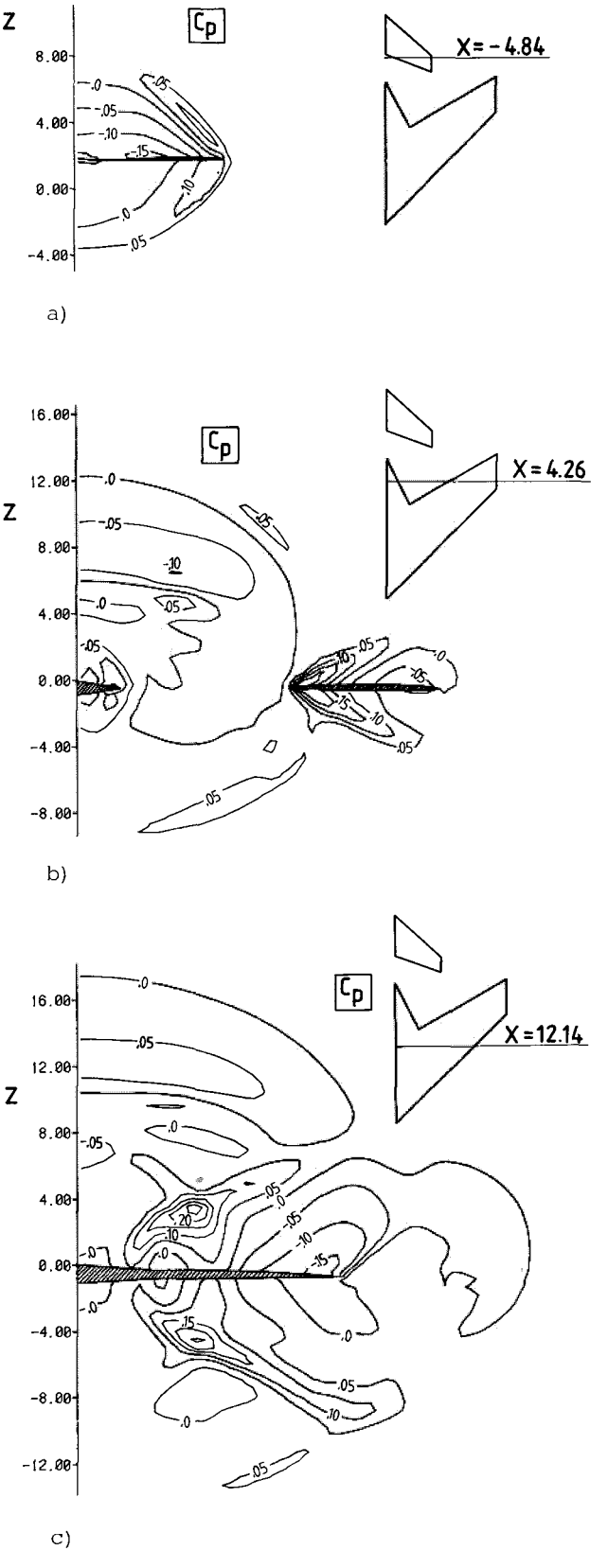

Fig 15. Isobar patterns in planes normal to free stream. M_∞=1.8, α=2°